Original Article

The effects of different factors on obstacle strength of irradiation defects: An atomistic study

Pan-dong Lin [a], Jun-feng Nie [b,*], Yu-peng Lu [a], Gui-yong Xiao [a], Guo-chao Gu [a], Wen-dong Cui [b], Lei He [b]

[a] Ministry of Education, Key Laboratory for Liquid-Solid Structural Evolution and Processing of Materials, School of Materials Science and Engineering, Shandong University, Jinan 250061, China
[b] Institute of Nuclear and New Energy Technology, Key Laboratory of Advanced Reactor Engineering and Safety of Ministry of Education, Tsinghua University, Beijing 100084, PR China

A B S T R A C T

In this work we study the effects of different factors of dislocation loop on its obstacle strength when interacting with an edge dislocation. At first, the interaction model for dislocation and dislocation loop is established and the full and partial absorption mechanism is obtained. Then, the effect of temperature, size and burgers vector of dislocation loop are investigated. The relation between the obstacle strength and irradiation dose has been established, which bridges the irradiation source and microscale properties. Except that, the obstacle strength of C, Cr, Ni, Mn, Mo and P decorated dislocation loop is studied. Results show that the obstacle strength for dislocation loop decorated by alloy element decreases in the sequence of Cr, Ni, Mn, C, P and Mo, which could be used to help parameterize and validate crystal plasticity finite element model and therein integrated constitutive laws to enable accounting for irradiation-induced chemical segregation effects.

1. Introduction

Reactor pressure vessel (RPV) is the most significant equipment in the nuclear power plant for the fact that it could not be replaced during the whole operating time [1]. Such being the case, the operation life and economy of the nuclear power plant is determined by RPV's service life [2]. High temperature, high pressure and strong irradiation are the typical characteristic of its harsh service environment. However, under irradiation, the deterioration of material properties occurs such as hardening, swelling and embrittlement [3,4]. From the physical standpoint, the irradiation-induced hardening and embrittlement is attributed to the fact that dislocation line which is related to the plastic deformation in metals are pinned by irradiation defects such as dislocation loops, stacking fault tetrahedral, voids and solute clusters [5–7] (see Table 3).

Numerous atomic simulations were performed to investigate the details of the dislocation-irradiation defect interactions. The research target is conventionally the BCC-Fe, which is considered as the basis for RPV steel. Furthermore, previous studies have suggested that dislocation loops are the major irradiation defects in metal materials. Such being the case, molecular dynamics method is used to reveal the interaction

mechanism between dislocation and dislocation loop. Y. N.Osetsky et al. [8] focused on the influence of temperature and the number of interstitial dislocation loop atoms on their interaction mechanism through MD method. The <100> dislocation loops are fixed at low temperatures, while at high temperatures (>300 K), they glide freely over dislocation loop, resulting in superjog on the dislocation. With the increase of the number of interstitial atoms, the unpinning stress increases obviously. Jia et al. [9] investigated the effects of interaction geometry on pinning strength induced by interstitial dislocation loop in BCC-Fe. Results showed that the pinning strength of $1/2<111>$ dislocation loop was 0.2–0.8, which is determined by the interaction geometries of dislocation loop. Liu et al. [10] used molecular dynamics simulations to elucidate the interactions between screw dislocations and self-interstitial dislocation loop in BCC-Fe. The junction mechanism and helical dislocation mechanism are proposed, respectively. All together, these studies have provided fundamental explanations for the interaction mechanism between dislocation and dislocation loop [11–13]. However, the relation between obstacle strength of dislocation loop and irradiation dose is still unclear. Besides that, in RPV steel, dislocation loop is referred as the strong sinks according to the associated migrating

* Corresponding author.
  E-mail address: niejf@tsinghua.edu.cn (J.-f. Nie).

solutes. Therefore, some MD simulations [14–16] were launched to investigate the interaction mechanism of alloy element enriched dislocation. Note that there is no systematic study on the effects of alloy elements which is of our concern.

In this work, we study the effects of different factors of dislocation loop on its obstacle strength when interacting with an edge dislocation. This work is organized as follows. Part 2 shows the methods used for the simulation following this introduction. Part 3.1 summarize the interaction process between dislocation and dislocation loop. Part 3.2 analyze the obstacle strength for 1/2<111> and <100> dislocation loop. Part 3.3 mainly focuses on the effect of alloy element on the obstacle strength. The work is finalized with conclusion in Part 4.

2. Methods

Molecular dynamics (MD) simulations were performed using the large-scale atomic/molecular massively parallel simulator (LAMMPS) [17]. In this work, the dislocation loop size ranging from 1.5 nm to 9.0 nm was considered. We have considered non-decorated dislocation loops, dislocation loops decorated by 5, 11, 22, 30 and 40 C, Cr, Mn, Mo, Ni and P atoms. Fe atoms on dislocation loop are replaced by alloy element atoms randomly. Forces and energetics were computed using the interatomic potentials by Mendelev et al. (EAM-type) for FeFe [18], Hepburn et al. (EAM-type) for FeC [19], Eich et al. (EAM-type) for FeCr [20], Young-Min et al. (MEAM-type) for FeMn [21], Wang et al. (MEAM-type) for FeMo [22], Wu et al. (MEAM-type) for FeNi [23] and Liem et al. (EAM-type) for FeP [24]. Thus, a total of 200 different conditions were studied. In addition, to obtain statistically meaningful results, each condition was simulated 5 times with different seeds for the temperature and solute distributions. As such, a total of 1000 different MD simulations were performed.

The model described by Osetsky and Bacon [25] are employed to investigated the 1/2<111> dislocation - dislocation loop interaction. An example of the box model is provided in Fig. 1. The x, y and z axes of the BCC-Fe simulation box are oriented along [111], [−1−12] and [1−10] directions, respectively. Periodic boundary conditions are applied along x and y directions. Along z, the box could be divided into 3 parts: The top and bottom parts are rigidly fixed which contains several atomic planes. The atoms in the inner region could move freely to realize the simulation. The MD simulations started by initializing the velocity of the relaxed atoms according to the Maxwell-Boltzmann distribution at the desired simulation temperature T under NPT ensemble. And then simulated under NVT ensemble with a shear load applied to the top part at a fixed strain rate $7 \times 10^7 \, s^{-1}$. More details could be seen in Ref. [26]. The box size was considered with volumes $24.7 \times 14.0 \times 14.8 \, nm^3$ containing about 440,000 atoms. The box is large enough to investigate the interaction mechanism. The straight dislocation was created along
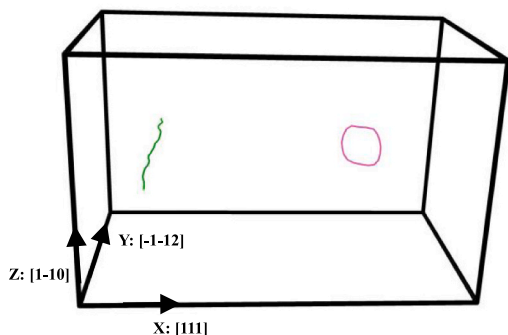
the y direction, parallel to the x axis. The dislocation loop was inserted in the center of box such that the glide plane of the dislocation cuts the dislocation loop at its center.

The open visualization tool (OVITO) [27,28] is used for all visualizations and dislocation analyses.

3. Results and discussion

3.1. Interaction process between dislocation and dislocation loop

1)The analysis of stress-strain curve

Fig. 2 presents the applied stress as function of the applied strain for [010] dislocation loop with 2.5 nm diameter at the temperature of 20 °C. Below is listed the interaction process briefly. The dislocation begun gliding along its glide plane when applied gilde force. Once the dislocation was near the dislocation, indicating their stress field interacted each other, the stress decreased to negative, which could be attributed to the fact that the dislocation movement induced plastic strain is larger than the imposed strain [29]. With the increase of strain, the dislocation loop could be seen as obstacle which pinned the dislocation and resist glide. So more shear stress is required for the dislocation to overcome obstruction interaction. Here, the shear stress for the dislocation to break away from dislocation is called the critical resolved shear stress (CRSS). Subsequently, the stress decreased rapidly. Except for the value of CRSS, the shape of stress curves are similar for varied dislocation loop at different temperature. Based on previous study [30], the value of CRSS is related to the size of simulation box, as a consequence of which, it could not make a comparison without the same box size. So in this study, obstacle strength is the main research target for it is independent for box size which is listed in next section.

2) Partial and full absorption reaction

Prior to describing the obstacle strength, we recall the interaction mechanism under the loading conditions applied here. Basically, the mechanism could be divided into two types: full and partial absorption reaction.

The full absorption reaction of a dislocation loop with $\boldsymbol{b} = 1/2<111>$ is reported in Refs. [8,31,32]. We take $\boldsymbol{b} = 1/2[−111]$ dislocation loop as an example. Fig. 3 shows the configuration evolution between 1/2[111] dislocation and 1/2[−111] dislocation loop with 5.0 nm diameter at 600 K. Note that dislocation loop is centered on the dislocation glide plane. At first, the formation of

Fig. 1. The box model to simulate the dislocation-dislocation loop interaction. The green line represents the 1/2<111> edge dislocation while the pink lines shows the <100> loop. (For interpretation of the references to colour in this figure legend, the reader is referred to the Web version of this article.)
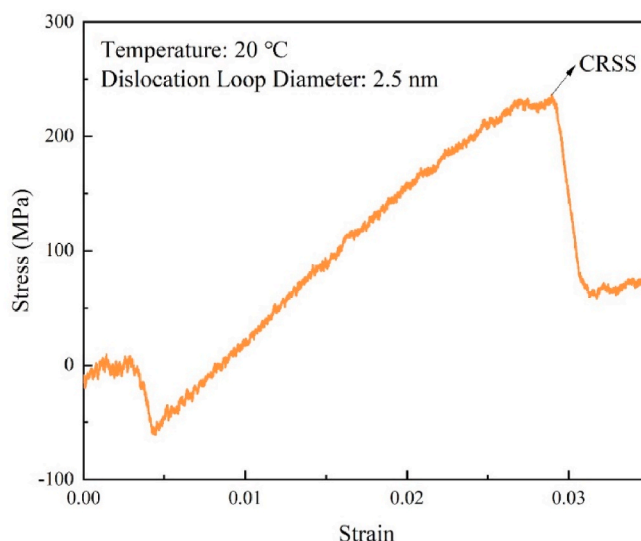

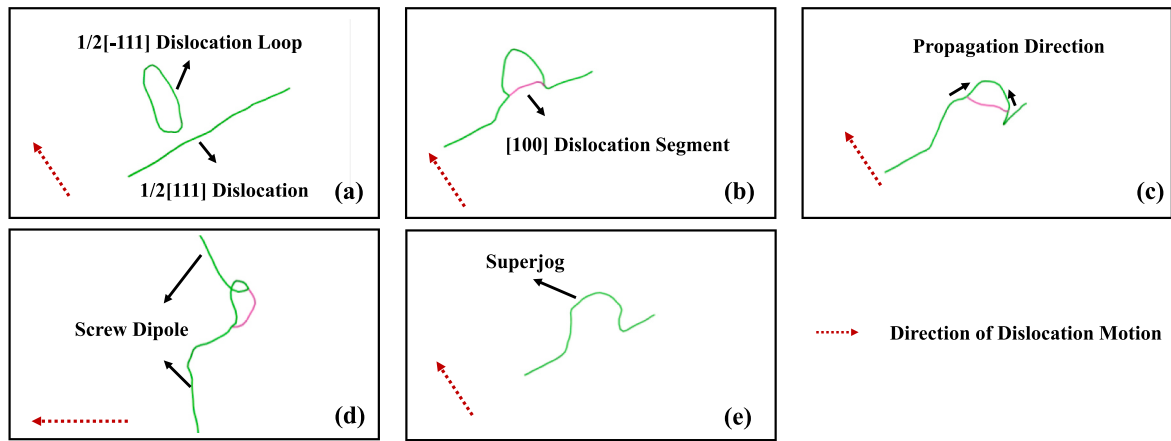**Fig. 2.** Stress-strain curves for [010] dislocation loop.

Fig. 3. Visualization of different stages of full absorption.

[100] reaction segment which pins the dislocation could be clearly found in Fig. 3(b) by the reaction of:

$$\frac{1}{2}[111] - \frac{1}{2}[-111] = [100] \tag{1.1}$$

With increasing stress, the [100] segment then glides across the loop surface and converts **b** of dislocation loop to 1/2[111] as shown in Fig. 3 (c) and the dislocation bows out until a screw dipole is formed as shown in Fig. 3(d), after which the dislocation loop is absorbed as a superjog on the dislocation. As have been noted above, the interaction mechanism requires the formation and propagation of a reaction segment of <100> type. It could be attributed to the fact that the migration energy of 1/2<111> dislocation loops is very small (about 0.05 eV) resulting in an athermal glide [31].

As for the <100> dislocation loop, several mechanisms occur which is based on their structure and orientation [33]. Here the case for partial absorption with **b** = [010] is considered where the dislocation loop is centered on the dislocation glide plane. Fig. 4 shows the different stages of partial absorption where the **b** of dislocation and dislocation loop is 1/2[111] and [010] respectively and loop diameter is 5.0 nm at 293 K The absorption reaction proceeds as follows. Due to the attraction of dislocation loop, the dislocation moves towards it and interacts with loop at Point A and B, respectively. Then it undergoes reaction to form

1/2 [1–11] dislocation segment immediately as show in Fig. 4(b). Then the latter propagates across the loop surface below dislocation slip plane, converting **b** to 1/2 [1–11] by the reaction as shown in Fig. 4(c) and (d):

$$\frac{1}{2}[111] - [010] = \frac{1}{2}[1-11] \tag{1.2}$$

Under increasing stress, dislocation line bows forward to create a screw dipole. Then the 1/2[111] segment glides across the loop surface left. Finally, the loop is absorbed as superjog on the 1/2[111] dislocation and a 1/2 [1–11] dislocation loop is formed in place of the original [010] loop. Note that the classification method of full- and partial-absorption dislocation loop at microscale is applied to the revision of the crystal plasticity finite element method (CPFEM) at mesoscale, which could be seen in our previous work [34].

3.2. Obstacle strength analysis

The aim of this section is to investigate the effect of temperature and diameter of dislocation loop on obstacle strength α. Its range is from 0 to 1.0 represents no additional stress required to break through the obstacle while 1 represents the obstacle by-passed by the dislocation. Generally, the definition of α reads:

$$\alpha = sin(\varphi_c) \tag{1.3}$$

This method calculates the obstacle strength by measuring the
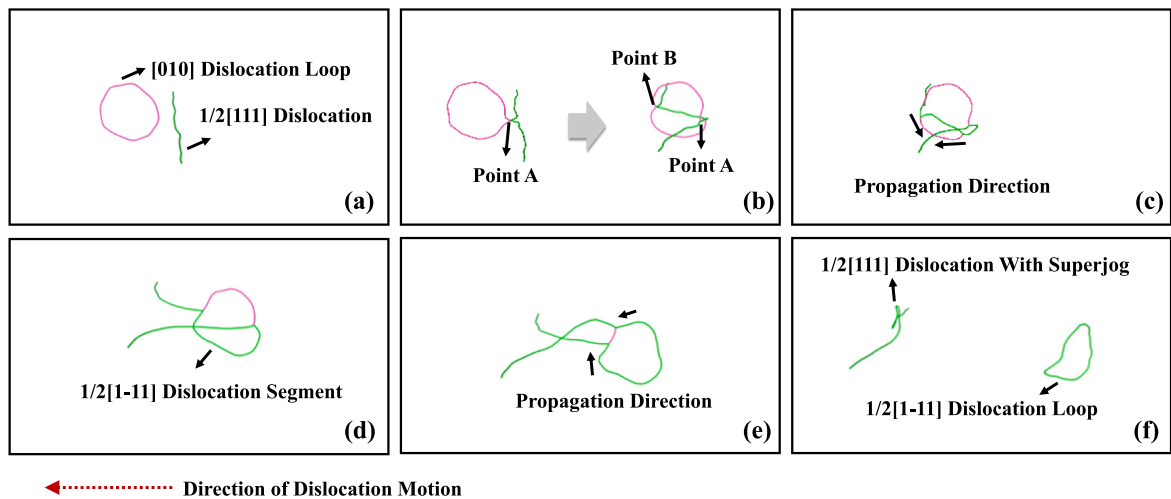

Fig. 4. Visualization of different stages of partial absorption.

critical Angle of the dislocation when the dislocation interacts with the dislocation loop, which is the most basic method of calculating the obstacle strength. When interacting with dislocation loop, dislocation would bow due to the force exerted by the dislocation loop. Such being the case, φ_c is the critical bowing angle at which the dislocation breaks away from dislocation loop. However, the critical bowing angle is hard to calculate accurately for the fact that the curvature of dislocation segments varies strongly surrounding the dislocation loop. So the obstacle strength could be analyzed qualitatively but not quantitatively through configuration pictures.

But based on the obstacle stress, the obstacle strength α could be obtained by the line tension model [35] which is equivalent to Eq (1.3):

$$\alpha = \frac{\tau_{obs}(L-d)}{\mu b} \tag{1.4}$$

where L is the box size along y axis, d is the diameter of dislocation loop, μ is the shear modulus of Fe and assumed to be 60 GPa, τ_{obs} is the obstacle stress which is defined as:

$$\tau_{obs} = \tau_C - \tau_f \tag{1.5}$$

where τ_c is the maximum shear stress when the dislocation interacts with dislocation, which is also named as critical resolved shearing stress and τ_f is the maximum shear stress when dislocation moving without dislocation loop. According to Bonny's research [30], When temperature is in the range of 300–750 K, τ_f is increases linearly with temperature. It could be read as:

$$\tau_f = 0.018 \cdot T + 6.59 \tag{1.6}$$

Note that obstacle strength is independent of box [30]. So it can be used as an inherent parameter to characterize the properties of dislocation loops. It is well known that irradiation could produce dislocation loop in Fe-based alloy and the average diameter of dislocation loop increasing with irradiation dose (dpa). According to our pervious study, the diameter of dislocation loop is in the power function relation with dpa for A508-III steel where the irradiation source is Fe ion.

The relationship between the diameter of dislocation loop and irradiation dose at 20 °C reads:

$$d(\text{nm}) = 3.23 \cdot \Phi^{0.48} \tag{1.7}$$

The relationship between the diameter of dislocation loop and irradiation dose at 100 °C reads:

$$d(\text{nm}) = 5.27 \cdot \Phi^{0.28} \tag{1.8}$$

The relationship between the diameter of dislocation loop and irradiation dose at 300 °C reads:

$$d(\text{nm}) = 8.70 \cdot \Phi^{0.23} \tag{1.9}$$

According to Eqs (1.7)-(1.9), the diameter of dislocation loop is converted into the irradiation dose dpa at the corresponding temperature, so as to facilitate the subsequent establishment of the relationship between the obstacle strength and irradiation dose dpa. There are 1/2<111> and <100> dislocation loop in BCC metals. Based on the study [36], the 1/2<111> dislocation loop accounted for 66 % while the number fraction of <100> dislocation loop is about 34 % in A508-III steel.

1) 1/2<111> dislocation loop

When it comes to 1/2<111> dislocation loop, the relationship between obstacle strength and the diameter of dislocation loop whose $\boldsymbol{b} = 1/2[-111]$ and which is centered in the dislocation glide plane could be obtained in Fig. 5. It could be seen that the obstacle strength tends to
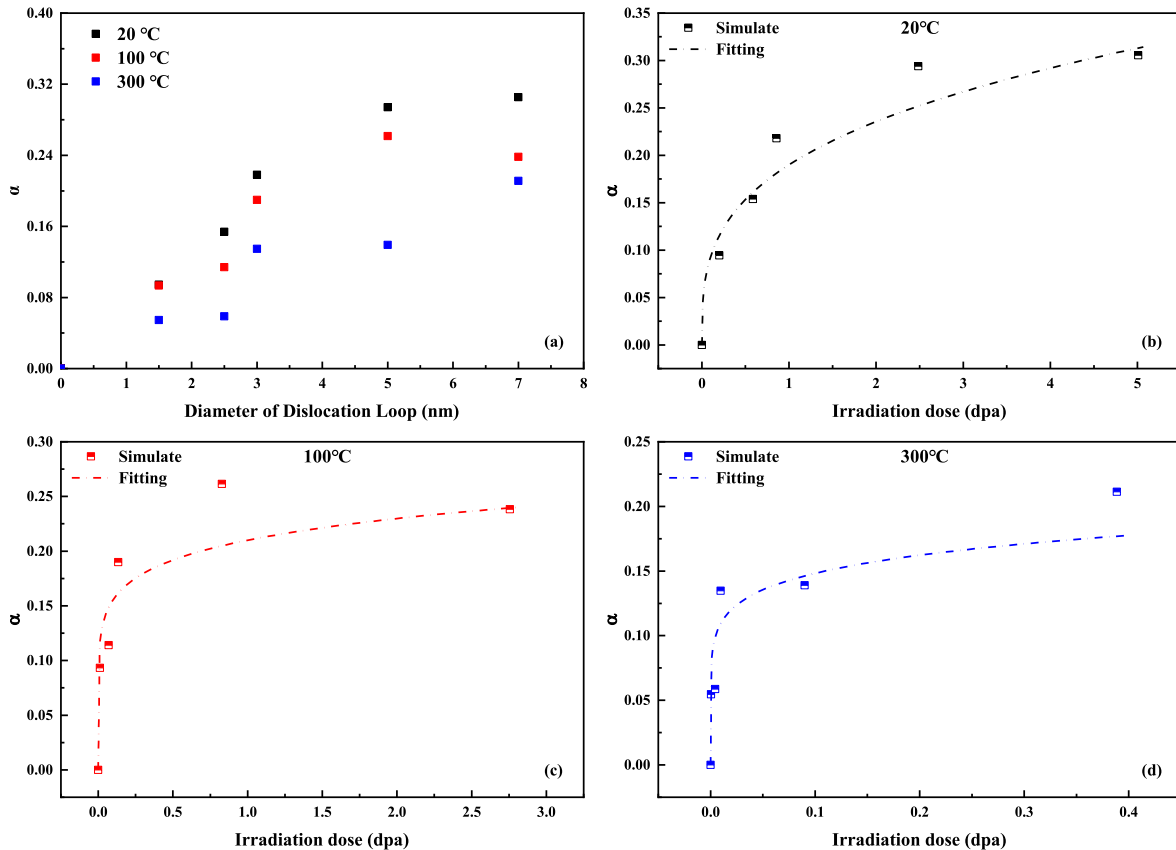

Fig. 5. (a)The relationship between α and diameter of dislocation loop with b = 1/2[−111] (b–d) The fitting curve of 1/2<111> dislocation loop obstacle strength and irradiation dose.

decrease systematically with the temperature. Depending on the dislocation loop size, the larger dislocation loop gives a higher strength. Based on this, obstacle strength could be in a power function relation with irradiation dose.

In order to facilitate the calculation of the average obstacle strength of 1/2<111> dislocation loops in A508-III steel at different irradiation doses dpa, the relationship between the defect strength and the irradiation dose dpa at three temperatures (20 °C, 100 °C, and 300 °C) were established.

The relationship between the obstacle strength and irradiation dose at 20 °C reads:

$$\alpha_{\frac{1}{2}\langle 111\rangle} = 0.19 \cdot \Phi^{0.31} \tag{1.10}$$

The relationship between the obstacle strength and irradiation dose at 100 °C reads:

$$\alpha_{\frac{1}{2}\langle 111\rangle} = 0.21 \cdot \Phi^{0.13} \tag{1.11}$$

The relationship between the obstacle strength and irradiation dose at 300 °C reads:

$$\alpha_{\frac{1}{2}\langle 111\rangle} = 0.20 \cdot \Phi^{0.13} \tag{1.12}$$

The fitting curve of 1/2<111> dislocation loop obstacle strength and irradiation dose dpa is shown in Fig. 5 (b)–(d).

2) <100> dislocation loop

When it comes to <100> dislocation loop, the relationship between obstacle strength and the diameter of dislocation loop whose b = [010] is shown in Fig. 6. It could be seen: (1) Temperature has negligible effect on defect strength. (2) The relation between α and dislocation loop diameter could be fitted to two straight lines. The obstacle strength decrease with the increasing loop diameter when diameter is less than 3 nm. Then the obstacle strength decreases with loop diameter.

During the interaction, the 1/2<111> dislocation segment will sweep the relevant <100> dislocation loop. The critical resolved shear stress is related to the sweep length of <100> dislocation segment. The longer the sweep length is, the higher critical resolved shear stress is. Fig. 6 (b) shows the process of dislocation-2nm < 0.100> dislocation loop interaction and dislocation-8nm < 0.100> dislocation loop interaction at 100 °C, when the diameter of dislocation loop is less than 3 nm, the 1/2<111> dislocation can sweep the entire <100> dislocation loop. Therefore, the increasing diameter leads to the longer sweep length and larger defect strength. When the diameter of dislocation loop is larger than 3 nm, 1/2<111> dislocation only sweeps the top half of <100> dislocation loop, forming a BI loop, it is unable to sweep the entire <100> dislocation loop. According to the definition of defect strength, the value of critical resolved shear stress remains unchanged, but the size of dislocation loop increases; such being the case, the defect strength decreases.

As mentioned in the obstacle strength analysis of 1/2<111> dislocation loop, obstacle strength could be in a power function relation with irradiation dose.

The critical irradiation dose for obstacle strength at 20 °C is 0.8574 dpa, and the relationship between the obstacle strength and irradiation dose at 20 °C reads:

$$\alpha_{\langle 100\rangle} = \begin{cases} 0.50 \cdot \Phi^{0.80} & \Phi \leq 0.8574 \\ 0.36 \cdot \Phi^{-0.35} & \Phi > 0.8574 \end{cases} \tag{1.13}$$

The critical irradiation dose for obstacle strength at 100 °C is 0.1337 dpa, and the relationship between the obstacle strength and irradiation dose at 100 °C reads:

$$\alpha_{\langle 100\rangle} = \begin{cases} 0.96 \cdot \Phi^{0.46} & \Phi \leq 0.1337 \\ 0.27 \cdot \Phi^{-0.19} & \Phi > 0.1337 \end{cases} \tag{1.14}$$
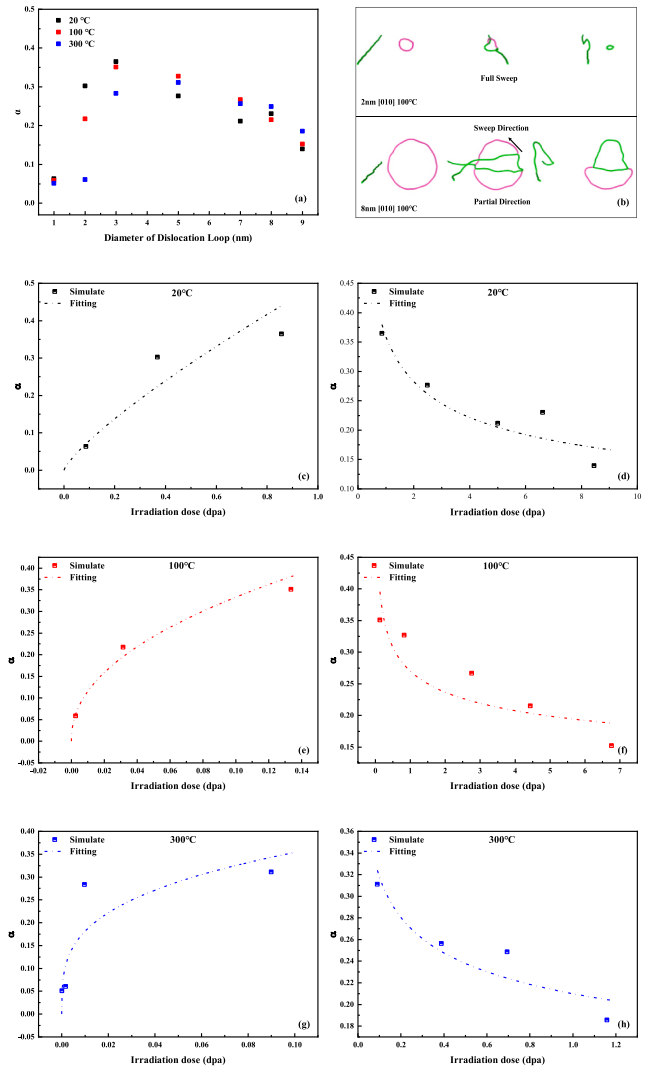

Fig. 6. (a) The relationship between α and diameter of dislocation loop with b = [010]. (b) The process of dislocation-2nm [010] dislocation loop interaction and dislocation-8nm [010] dislocation loop interaction at 100 °C. (c)–(h) The fitting curve of 1/2<111> dislocation loop obstacle strength and irradiation dose.

The critical irradiation dose for obstacle strength at 300 °C is 0.0900 dpa, and the relationship between the obstacle strength and irradiation dose at 300 °C reads:

$$\alpha_{\langle 100\rangle} = \begin{cases} 0.69 \cdot \Phi^{0.29} & \Phi \leq 0.0900 \\ 0.21 \cdot \Phi^{-0.18} & \Phi > 0.0900 \end{cases} \tag{1.15}$$

The fitting curve of <100> dislocation loop obstacle strength and irradiation dose dpa is shown in Fig. 6(c).

The relation between the obstacle strength and irradiation dose has been established, which bridges the irradiation source and microscale properties. The dislocation loop investigated by molecular dynamics method is in BCC-Fe. However, many alloy elements are considered in A508-III steel which can also affect the results. Generally, the alloy elements in solution state are mainly related to σ_f, while alloy elements segregated at loop may affect the interaction between dislocation and dislocation loop. For example, Cr segregation could increase difficulty for dislocation to break away from loop. It is necessary to further study the effect of alloy elements on the obstacle strength.

3.3. The effect of alloy elements on obstacle strength

The main conclusions of this work are that depending on the specific Burgers vector, loop size and temperature, many different reactions occur leading to different levels of absorption and obstacle strength. In addition, due to statistical fluctuations, the same configuration may lead to different levels of absorption and different reconstruction of the remaining loops. Clearly, addressing all possible configurations in the scope of the effect of alloy elements is not manageable. So in this part, we mainly focus on the effects of alloy elements on obstacle strength and absorption type. Apart from that, we have considered non-decorated loops, loops decorated by 5, 11, 22, 30 and 40 atoms for C, Cr, Mn, Ni, Mo and P element, respectively. For specific number of decorated atoms, three different configurations are considered.

Fig. 7(a) and (b) shows the effect of alloy elements on obstacle strength. It could be concluded that: (1) The elements of C, Cr, Mn and Ni increases the obstacle strength. As for the case of C and Ni, the obstacle strength is positive to the number of decorated alloy atoms. In contrast, obstacle strength decreases with increasing decorated alloy atoms for case Mn. The effect of the number of decorated alloy atoms is negligible for case Cr. (2) In terms of case Mo, the obstacle strength for the dislocation loop decorated by Mo is smaller than that without Mo element. (3) When it comes to the case of P, alloy element P whose number is 5 and 11 decreases the obstacle strength and strengthens α whose number is 22, 30 and 40. (4) Generally, the obstacle strength for dislocation loop decorated by alloy element decreases in the sequence of Cr, Ni, Mn, C, P and Mo. (5) Changes in the number of Ni, Cr, Mn, Mo atoms have little influence on α, α hardly varies with the number of these four atoms, but it increases significantly with the increase of C, P atoms.

Fig. 7 (c) shows the interaction process of 3 nm < 100> dislocation loop containing 22 C atoms with dislocation at 300 °C. (i) Before the interaction, C atoms are randomly distributed around the dislocation loop. (ii) During the interaction, enrichment of C atoms occurs at both pinning points of the dislocation loop on the dislocation, indicating that C atoms act as pinning points to make the dislocation pinned. (iii) After

the interaction, some C atoms are also sporadically distributed above the dislocation loop. This phenomenon is also observed in other elements.

As for 3 nm non-decorated $1/2<111>$ dislocation loop, the absorption process is a thermally activated process with an obstacle strength of 0.21 at 300 K. Below is listed the simplified interaction mechanism (Besides, all details could be seen in Ref. [37].). (i) At the moment of initial interaction, a reaction segment is created and the dislocation starts to bow out. (ii) In a second step, the reaction segment glides via thermal activation across the dislocation loop habit plane. (iii) Finally, it could be divided into two cases. If the propagation of the reaction segment is hindered, a screw dipole is drawn and when it closes a bypass reaction is realized leaving a (partial/restructured) dislocation loop behind. In the other case, the dislocation loop is fully absorbed as a (double) super jog on the dislocation loop line. In this study, 3 nm non-decorated $1/2<111>$ dislocation loop is fully absorbed. However, the change of absorption type indeed occurs with the effects of alloy elements. The dislocation length of the dislocation before and after interaction with the dislocation loop is different. The difference could be compared to the reference cases where full absorption occurs with the aim of determining the level absorption. The absorption ratio for partial absorption is defined as the dislocation length of the dislocation before and after interaction divided by the dislocation length for full absorption cases for the fact that the loop reconstruction after interaction with dislocation hinders direct observation of the remaining dislocation length of the dislocation loop. Table 1 shows the effects of type and number of decorated alloy atoms at 3 nm dislocation loop on the reaction type and absorption ratio. Further, we observe that the interaction

Table 1
CRSS of the dislocation-1/2[−111] dislocation loop interaction.

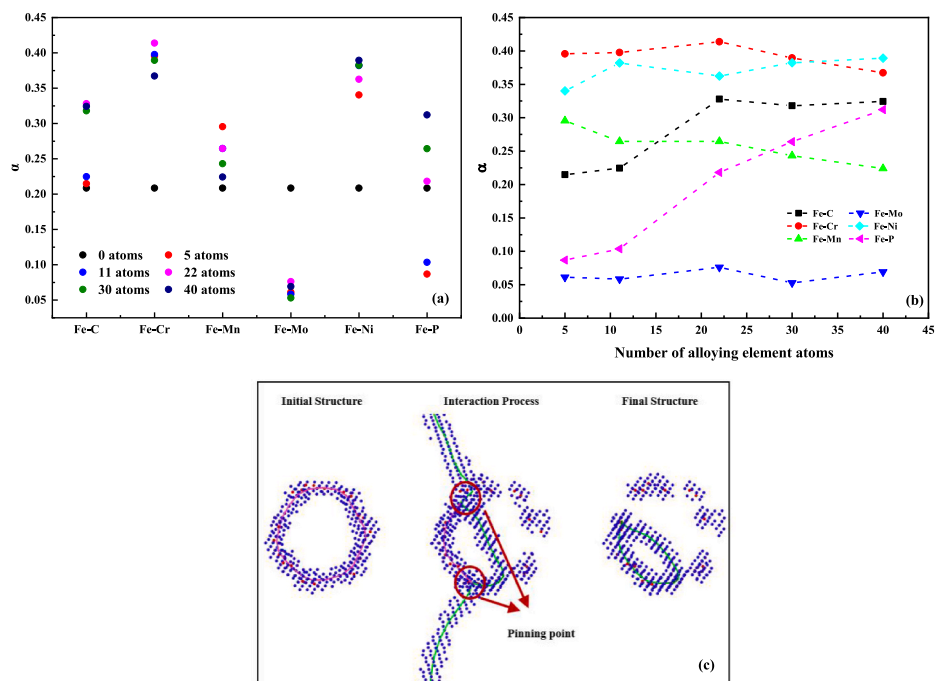| (MPa)	1.5 nm	2.5 nm	3 nm	5 nm	7 nm
20 °C	123.70	210.35	305.97	496.72	659.21
100 °C	124.11	160.45	269.45	444.45	518.22
300 °C	81.71	92.69	198.72	246.11	464.66

Fig. 7. (a) The effect of alloy elements on obstacle strength. (b) The relationship between obstacle strength and the number of alloy atoms. (c) The interaction process of dislocation and <100> dislocation loop decorated by 22 C atoms.

Table 2

CRSS of the dislocation [010] dislocation loop interaction.

(MPa)	1 nm	2 nm	3 nm	5 nm	7 nm	8 nm	9 nm
20 °C	84.00	385.62	503.64	467.69	460.45	581.47	426.29
100 °C	80.34	282.11	486.28	552.35	578.78	544.76	464.76
300 °C	75.13	91.79	399.07	529.58	560.14	631.79	567.91

Table 3

CRSS for different segregation fracture.

(MPa)	3.88 % (5/129 atoms)	8.53 % (11/129 atoms)	17.05 % (22/129 atoms)	23.26 % (30/129 atoms)	31.01 % (40/129 atoms)
Fe–C	301.84	314.92	454.35	440.91	449.35
Fe–Cr	545.45	548.39	569.91	537.18	507.25
Fe–Mn	410.49	368.68	368.77	339.92	314.24
Fe–Mo	94.52	90.76	114.66	83.46	105.22
Fe–Ni	470.92	527.14	500.94	527.74	537.06
Fe–P	128.95	151.72	306.30	368.32	432.81

mechanism between dislocation and dislocation does change by solute enrichment to some extent. When the 3 nm $<100>$ dislocation loops are not decorated, dislocation loops are fully absorbed, but when the dislocation loops are decorated, the absorption of dislocation loops changes significantly. The solutes of C, Cr Mn, Ni and P hinder the mobility of the reaction segment leading to partial absorption with increasing obstacle strength compared with non-decorated dislocation loop. Among them, two non-metallic elements, C and P, have significant effects compared to three metallic elements, Cr Mn Ni. In contrast, it could be seen that the cloud of solutes significantly decreases the resistance for dislocation to break away from dislocation loop. Hence, the full absorption is observed for all investigated Mo cases regardless of the number of decorated atoms (see Table 2).

Fig. 8 shows the effect of temperature on obstacle strength for 3 nm $1/2<111>$ dislocation loop decorated by C atoms (see Table 4). The decoration of the dislocation loop by C has a large impact on α with strong temperature dependence: the increasing temperature leads to decreasing obstacle strength. The temperature behavior associated to α for C enriched dislocation loops is consistent with its behavior associated to the absorbed fraction of the dislocation loop. As shown in Table 5, the cases for full absorption occurs more frequently with increasing temperature, which is consistent with previous work [15,30] (see Table 6).
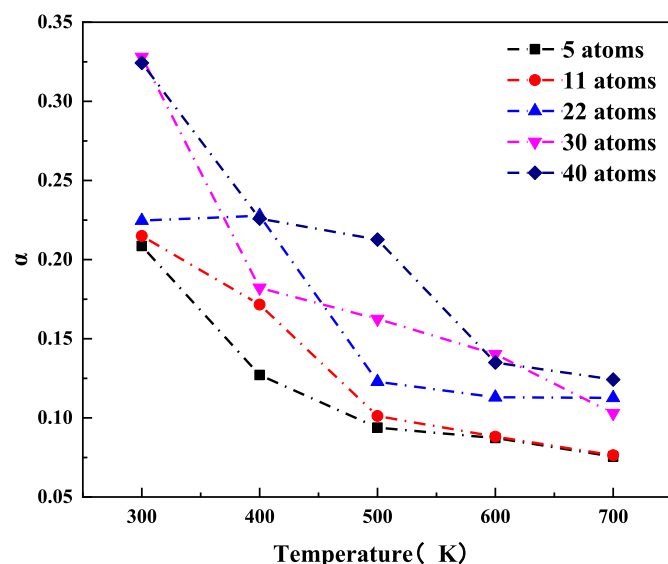
Table 4

Summary of the obtained results for varied alloy elements.

	5 atoms	11 atoms	22 atoms	30 atoms	40 atoms
C	3/3 Full absorption	2/3 Full absorption Absorption Ratio: 18 %	1/3 Full absorption Absorption Ratio: 6 %/14 %	1/3 Full absorption Absorption Ratio: 20 %/15 %	1/3 Full absorption Absorption Ratio: 54 %/2 %
Cr	1/3 Full absorption Absorption Ratio: 50 %/85 %	3/3 Full absorption	2/3 Full absorption Absorption Ratio: 10 %	3/3 Full absorption	2/3 Full absorption Absorption Ratio: 80 %
Mn	2/3 Full absorption Absorption Ratio: 64 %	2/3 Full absorption Absorption Ratio: 49 %	3/3 Full absorption	3/3 Full absorption	3/3 Full absorption
Mo	3/3 Full absorption	3/3 Full absorption	3/3 Full absorption	3/3 Full absorption	3/3 Full absorption
Ni	1/3 Full absorption Absorption Ratio: 47 %/92 %	2/3 Full absorption Absorption Ratio: 74 %	2/3 Full absorption Absorption Ratio: 70 %	0/3 Full absorption Absorption Ratio: 66 %/72 %/58 %	1/3 Full absorption Absorption Ratio: 66 %/46 %
P	3/3 Full absorption	3/3 Full absorption	2/3 Full absorption Absorption Ratio: 10 %	1/3 Full absorption Absorption Ratio: 71 %/24 %	1/3 Full absorption Absorption Ratio: 16 %/16 %

Table 5

CRSS for different temperature.

(MPa)	3.88 % (5/129 atoms)	8.53 % (11/129 atoms)	17.05 % (22/129 atoms)	23.26 % (30/129 atoms)	31.01 % (40/129 atoms)
300 K	293.30	301.84	314.92	454.35	449.35
400 K	185.22	245.22	320.99	259.48	318.41
500 K	142.06	152.06	181.22	234.73	302.40
600 K	135.07	136.19	169.80	206.54	199.44
700 K	121.14	122.21	171.15	158.06	186.73

4. Conclusions

We have studied the effects of the specific Burgers vector, loop size alloy element and temperature on obstacle strength of dislocation loop when interacting with $1/2 <111>$ edge dislocation by molecular dynamics method. The interaction model for dislocation and dislocation loop is established and the full and partial absorption mechanism is obtained.

➢ As for $1/2 <111>$ dislocation loop, the obstacle strength tends to decrease systematically with the temperature. Depending on the dislocation loop size, the larger dislocation loop gives a higher strength. Furthermore, obstacle strength could be in a power function relation with irradiation dose.

Fig. 8. The effect of temperature on obstacle strength.

Table 6
Summary of the obtained results for varied temperature.

	5 atoms	11 atoms	22 atoms	30 atoms	40 atoms
300 K	3/3 Full absorption	2/3 Full absorption Absorption Ratio: 18 %	1/3 Full absorption Absorption Ratio: 6 %/14 %	1/3 Full absorption Absorption Ratio: 20 %/15 %	1/3 Full absorption Absorption Ratio: 54 %/2 %
400 K	3/3 Full absorption	2/3 Full absorption Absorption Ratio: 9 %	2/3 Full absorption Absorption Ratio: 9 %	3/3 Full absorption	3/3 Full absorption
500 K	3/3 Full absorption	3/3 Full absorption	3/3 Full absorption	3/3 Full absorption	3/3 Full absorption
600 K	3/3 Full absorption	3/3 Full absorption	3/3 Full absorption	3/3 Full absorption	3/3 Full absorption
700 K	3/3 Full absorption	3/3 Full absorption	3/3 Full absorption	3/3 Full absorption	3/3 Full absorption

➤ In terms of <100> dislocation loop, temperature has negligible effect on defect strength. The obstacle strength decrease with the increasing loop diameter when diameter is less than 3 nm. Then the obstacle strength decreases with loop diameter.

➤ As for the effect of alloy elements on obstacle strength, the elements of C, Cr, Mn and Ni increases the obstacle strength. Furthermore, the obstacle strength for the dislocation loop decorated by Mo is smaller than that without Mo element. When it comes to the case of P, alloy element P whose number is 5 and 11 decreases the obstacle strength and strengthens α whose number is 22, 30 and 40.

➤ The interaction mechanism between dislocation and dislocation does change by solute enrichment. The solutes of C, Cr Mn, Ni and P hinder the mobility of the reaction segment leading to partial absorption with increasing obstacle strength compared with non-decorated dislocation loop. In contrast, the full absorption is observed for all investigated Mo cases regardless of the number of decorated atoms.

CRediT authorship contribution statement

Pan-dong Lin: Conceptualization, Formal analysis, Investigation, Methodology, Validation, Visualization, Data curation, Writing –original draft, Writing – review & editing. **Jun-feng Nie**: Funding acquisition, Resources, Software, Conceptualization, Methodology, Project administration, Supervision, Validation, Writing – review & editing. **Yu-peng Lu, Gui-yong Xiao, Guo-chao Gu, Wen-dong Cui and Lei He:** Data curation.

Data availability

All the data that support the findings of this study are available upon reasonable request.

Declaration of competing interest

The authors declare that they have no known competing financial interests or personal relationships that could have appeared to influence the work reported in this paper.

Acknowledgements

Appendix A. Comparison of effect of strain rate and potential

For the effect of strain rate on simulation results, the strain rate in the manuscript is 7×10^7 s^{-1}, and two strain rates of 3.5×10^7 s^{-1} and 7×10^6 s^{-1} are selected as supplementary simulations. As shown in Fig. 9, changing the strain rate has little effect on the CRSS, and the error in the CRSS calculated using the three strain rates is 16.37 MPa, proving that our simulation is strain rate independent. The effect of strain rate is consistent with the work of Ref. [38]. For the effect of potentials on simulation results, the potential used for interaction simulation in pure Fe in the manuscript was developed by Mendelev [18] (Potential 1), and now we selected other 2 potentials developed by Byggmästar [39] (Potential 2) and Malerba [40] (Potential 3) for supplementary simulations. As shown in Fig. 10, changing potentials also has little effect on the CRSS, the error in the CRSS calculated using the three strain rates is 19.34 MPa. Overall, our simulation results are reliable.
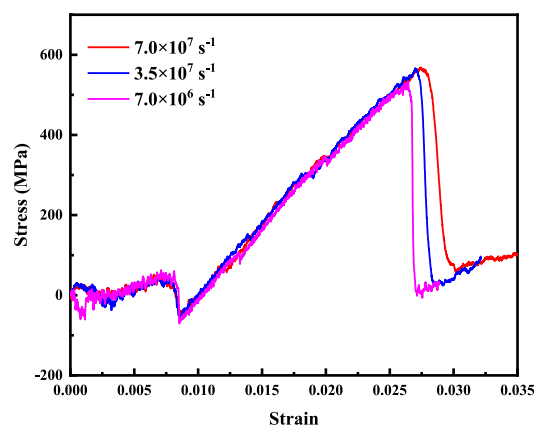

Fig. 9. Stress-strain curve of different strain rates (interaction with 3 nm [010] dislocation loop at 300K).
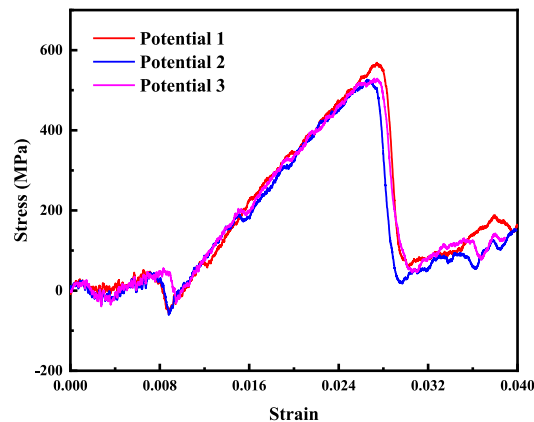
Fig. 10. Stress-strain curve of different potentials (interaction with 3 nm [010] dislocation loop at 300K).

References

[1] C. Li, G. Shu, W. Liu, Y. Duan, Effects of neutron irradiation on elastic modulus of RPV steel, Ann. Nucl. Energy 134 (2019) 20–26.

[2] J.C. Van Duysen, G. Meric De Bellefon, 60th Anniversary of electricity production from light water reactors: historical review of the contribution of materials science to the safety of the pressure vessel, J. Nucl. Mater. 484 (2017) 209–227.

[3] G.R. Odette, G.E. Lucas, Embrittlement of nuclear reactor pressure vessels, JOM 53 (7) (2001) 18–22.

[4] C.L. Li, G.G. Shu, B. Xu, Y. Liu, J. Chen, W. Liu, Effects of neutron irradiation on magnetic properties of reactor pressure vessel steel, Nucl. Eng. Des. 342 (2019) 128–132.

[5] H. Trinkaus, B.N. Singh, A.J.E. Foreman, Segregation of cascade induced interstitial loops at dislocations: possible effect on initiation of plastic deformation, J. Nucl. Mater. 251 (1997) 172–187.

[6] B.N. Singh, A.J.E. Foreman, H. Trinkaus, Radiation hardening revisited: role of intracascade clustering, J. Nucl. Mater. 249 (2–3) (1997) 103–115.

[7] S.A. Fabritsiev, A.S. Pokrovsky, Effect of irradiation temperature on microstructure, radiation hardening and embrittlement of pure copper and copper-based alloy, J. Nucl. Mater. 367 (2007) 977–983.

[8] D.J. Bacon, Y.N. Osetsky, Z. Rong, Computer simulation of reactions between an edge dislocation and glissile self-interstitial clusters in iron, Phil. Mag. 86 (25–26) (2006) 3921–3936.

[9] L.X. Jia, X.F. He, Y.K. Dou, D.J. Wang, S. Wu, H. Cao, W. Yang, The effects of interaction geometry on pinning strength induced by interstitial dislocation loop in BCC-Fe, Nucl. Instrum. Methods Phys. Res. Sect. B Beam Interact. Mater. Atoms 456 (2019) 103–107.

[10] X.Y. Liu, S.B. Biner, Molecular dynamics simulations of the interactions between screw dislocations and self-interstitial clusters in body-centered cubic Fe, Scripta Mater. 59 (1) (2008) 51–54.

[11] D. Terentyev, M. Klimenkov, L. Malerba, Confinement of motion of interstitial clusters and dislocation loops in BCC Fe–Cr alloys, J. Nucl. Mater. 393 (1) (2009) 30–35.

[12] B. Gómez-Ferrer, C. Dethloff, E. Gaganidze, L. Malerba, C. Hatzoglou, C. Pareige, Nano-hardening features in high-dose neutron irradiated Eurofer97 revealed by atom-probe tomography, J. Nucl. Mater. 537 (2020).

[13] F. Bergner, C. Pareige, V. Kuksenko, L. Malerba, P. Pareige, A. Ulbricht, A. Wagner, Critical assessment of Cr-rich precipitates in neutron-irradiated Fe–12at%Cr: comparison of SANS and APT, J. Nucl. Mater. 442 (1–3) (2013) 463–469.

[14] A.V. Bakaev, D.A. Terentyev, E.E. Zhurkin, Effect of segregation of Ni and Cr at dislocation loops on their interaction with gliding dislocations in irradiated Fe-Ni-Cr BCC alloys, J. Surf. Ingestig. 12 (4) (2018) 783–791.

[15] D. Terentyev, A. Bakaev, E.E. Zhurkin, Effect of carbon decoration on the absorption of ⟨100⟩ dislocation loops by dislocations in iron, J. Phys. Condens. Matter 26 (16) (2014) 165402.

[16] D. Terentyev, X. He, G. Bonny, A. Bakaev, E. Zhurkin, L. Malerba, Hardening due to dislocation loop damage in RPV model alloys: role of Mn segregation, J. Nucl. Mater. 457 (2015) 173–181.

[17] S. Plimpton, Fast parallel algorithms for short-range molecular dynamics, J. Comput. Phys. 117 (1) (1995) 1–19.

[18] M.I. Mendelev, S. Han, D.J. Srolovitz, G.J. Ackland, D.Y. Sun, M. Asta, Development of new interatomic potentials appropriate for crystalline and liquid iron, Philos. Mag. A 83 (35) (2003) 3977–3994.

[19] D.J. Hepburn, G.J. Ackland, Metallic-covalent interatomic potential for carbon in iron, Phys. Rev. B 78 (16) (2008).

[20] S.M. Eich, D. Beinke, G. Schmitz, Embedded-atom potential for an accurate thermodynamic description of the iron–chromium system, Comput. Mater. Sci. 104 (2015) 185–192.

[21] Y.-M. Kim, Y.-H. Shin, B.-J. Lee, Modified embedded-atom method interatomic potentials for pure Mn and the Fe–Mn system, Acta Mater. 57 (2) (2009) 474–482.

[22] J. Wang, H. Kwon, H.S. Kim, B.-J. Lee, A neural network model for high entropy alloy design, npj Comput. Mater. 9 (1) (2023).

[23] C. Wu, B.-J. Lee, X. Su, Modified embedded-atom interatomic potential for Fe-Ni, Cr-Ni and Fe-Cr-Ni systems, Calphad 57 (2017) 98–106.

[24] H. Liem, J. Cabanillas-Gonzalez, P. Etchegoin, D.D.C. Bradley, Glass transition temperatures of polymer thin films monitored by Raman scattering, J. Phys. Condens. Matter 16 (6) (2004) 721–728.

[25] Y.N. Osetsky, D.J. Bacon, An atomic-level model for studying the dynamics of edge dislocations in metals, Model. Simulat. Mater. Sci. Eng. 11 (4) (2003) 427.

[26] P. Lin, J. Nie, M. Liu, Molecular dynamics study of the interactions between the 1/2 [-1-11] edge dislocation and the [010] dislocation loop in BCC-Fe, J. Tsinghua Univ. (Sci. Technol.) 62 (12) (2022) 1.

[27] A. Stukowski, Visualization and analysis of atomistic simulation data with OVITO–the Open Visualization Tool, Model. Simulat. Mater. Sci. Eng. 18 (1) (2010).

[28] A. Stukowski, V.V. Bulatov, A. Arsenlis, Automated identification and indexing of dislocations in crystal interfaces, Model. Simulat. Mater. Sci. Eng. 20 (8) (2012) 085007.

[29] D.J. Bacon, Y.N. Osetsky, Mechanisms of hardening due to copper precipitates in α-iron, Phil. Mag. 89 (34–36) (2009) 3333–3349.

[30] G. Bonny, A. Bakaev, D. Terentyev, The combined effect of carbon and chromium enrichment on (100) loop absorption in iron, Comput. Mater. Sci. 211 (2022) 8.

[31] Z. Rong, Y.N. Osetsky, D.J. Bacon, A model for the dynamics of loop drag by a gliding dislocation, Phil. Mag. 85 (14) (2005) 1473–1493.

[32] D. Terentyev, Y.N. Osetsky, D.J. Bacon, Competing processes in reactions between an edge dislocation and dislocation loops in a body-centred cubic metal, Scripta Mater. 62 (9) (2010) 697–700.

[33] D. Terentyev, P. Grammatikopoulos, D.J. Bacon, Y.N. Osetsky, Simulation of the interaction between an edge dislocation and a ⟨100⟩ interstitial dislocation loop in alpha-iron, Acta Mater. 56 (18) (2008) 5034–5046.

[34] P.D. Lin, J.F. Nie, M.D. Liu, Multiscale crystal plasticity finite element model for investigating the irradiation hardening and defect evolution mechanism of A508-3 steel, Nucl. Mater. Energy 32 (2022) 16.

[35] D.J. Bacon, Y.N. Osetsky, D. Rodney, Dislocation-obstacle interactions at the atomic level, in: J.P. Hirth, L. Kubin (Eds.), Dislocations in Solids, vol. 15, Elsevier Science Bv, Amsterdam, 2009, pp. 1–90.

[36] Q. Wan, G. Shu, R. Wang, H. Ding, X. Peng, Q. Zhang, J. Lei, Study on the microstructure evolution of A508-3 steel under proton irradiation, Acta Metall. Sin. 48 (8) (2012) 929.

[37] G. Bonny, D. Terentyev, J. Elena, A. Zinovev, B. Minov, E.E. Zhurkin, Assessment of hardening due to dislocation loops in bcc iron: overview and analysis of atomistic simulations for edge dislocations, J. Nucl. Mater. 473 (2016) 283–289.

[38] D. Terentyev, L. Malerba, D.J. Bacon, Y.N. Osetsky, The effect of temperature and strain rate on the interaction between an edge dislocation and an interstitial dislocation loop in α-iron, J. Phys.-Condes. Matter 19 (45) (2007) 13.

[39] J. Byggmästar, F. Granberg, Dynamical stability of radiation-induced C15 clusters in iron, J. Nucl. Mater. 528 (2020) 6.

[40] L. Malerba, M.C. Marinica, N. Anento, C. Björkas, H. Nguyen, C. Domain, F. Djurabekova, P. Olsson, K. Nordlund, A. Serra, D. Terentyev, F. Willaime, C.

S. Becquart, Comparison of empirical interatomic potentials for iron applied to radiation damage studies, J. Nucl. Mater. 406 (1) (2010) 19–38.